Generation 2 of the ACME EDM Search

A. D. West and D. DeMille
Department of Physics, Yale University, 217 Prospect Street, New Haven, Connecticut 06511, USA

E. Kirilov
Institut für Experimentalphysik, Universität Innsbruck, Technikerstrasse 25/4, A-6020 Innsbruck, Austria

J. Doyle and G. Gabrielse
Department of Physics, Harvard University, 17 Oxford Street, Cambridge, Massachusetts 02138, USA
(Dated: March 29, 2017)

The ACME search for the electric dipole moment of the electron (eEDM) recently improved the associated upper limit by an order of magnitude [1]. This paper describes a set of upgrades that are projected to lead to another order of magnitude increase in statistical sensitivity. The main features include electrostatic focussing of the molecule beam, coherent state preparation via STIRAP, and an improved rotational cooling scheme. Important general considerations regarding their implementation are discussed, and their efficacy is illustrated through simulation and preliminary tests. Most of the proposed techniques borrow from other atomic and molecular physics experiments, and could be usefully implemented in other EDM searches.

I. INTRODUCTION.

The existence of a non-zero electron electric dipole moment (eEDM) implies violation of parity (P) and time-reversal (T) symmetries [2]. The standard model of particle physics predicts an eEDM, $d_e < 10^{-38}\ e\cdot\text{cm}$ [3]. Extensions to the standard model, such as Supersymmetric theories, often introduce additional T-violating interactions, and generally predict an eEDM value in the range 10^{-27}-$10^{-32}\ e\cdot\text{cm}$ (CITATION?).

The ACME collaboration recently published the best limit on the eEDM [1], achieved in an experiment using a beam of thorium monoxide (ThO) molecules. ThO has one of the largest known internal effective electric fields, $\mathcal{E}_{\text{eff}} \approx 75$ GV/cm of any dipolar molecule, and has a long-lived ($\tau \sim 2$ ms) paramagnetic state H with $(\sigma\delta)$ $^3\Delta_1$ configuration and term. This structure provides one relativistic σ-electron to produce the high $\mathcal{E}_{\text{eff}}$ and one δ-electron which gives rise to a small Ω-doubling. The latter provides an important additional 'switch' for effective suppression of systematic effects. Because of cancellation between the spin and orbital magnetic moments, the $^3\Delta_1$ state also possesses an extremely small g-factor $g \approx g_L\Lambda - g_S\Sigma \approx 0.008$ [4] which makes it very insensitive to magnetic field noise. ThO can also be efficiently produced by a cryogenic buffer-gas-cooled beam source, providing an increase in flux over conventional effusive or supersonic beams of over two orders of magnitude [5].

The statistical uncertainty, δd_e of the eEDM measurement scales as $d_e \propto S^{-1/2}$, where S is the measured signal. In this paper we present several methods which, when combined, we anticipate will provide a large overall increase in S compared to the current version of the experiment. We refer to the current version of the experiment as 'Generation 1' and the intended experimental configuration for our next reported measurement as 'Generation 2'. Gen. 1 of the experiment demonstrated a sensitivity of $\delta_e \approx 10^{-28}\ e\cdot\text{cm}/\sqrt{\text{day}}$. As detailed in this paper we anticipate that Gen. 2 will improve this sensitivity by an order of magnitude. Together with appropriate suppression and understanding of present systematic errors, and a comparable integration time, such an improvement will very stringently confine a number or standard model extensions.

In Section II we provide a brief overview of the experimental procedure used in Gen. 1, and outline the main changes we plan to implement. In Section III we describe these changes in detail, discuss the associated considerations, and present the results of initial experimental tests of these methods.

We also consider further improvements which are either beyond the anticipated scope of Gen. 2 or where the anticipated signal improvement is small or uncertain.

II. EXPERIMENTAL OVERVIEW

A. Gen. 1

The experimental apparatus used in Gen. 1 is illustrated schematically in Figure 1. The experiment begins with a cryogenic buffer gas beam source [5, 6]. A pulsed NdYAG laser ablates a ThO_2 ceramic precursor target inside a cell cooled to a temperature of around 15 K. The resulting plume of ThO molecules becomes entrained by inflowing neon buffer gas and exits an aperture in the cell. Thermalisation continues for a short distance after the cell, thus forming an effective source downstream. After 2.5 cm the molecules pass through a conical collimating aperture with a mean forward velocity, $v \approx 180$ m/s. We assume thermalisation to be complete by this point, an assumption supported by calculations based on a 'sudden freeze' model, and experimental evidence [7]. The rotational temperature is ≈ 4 K, with over 95% of the

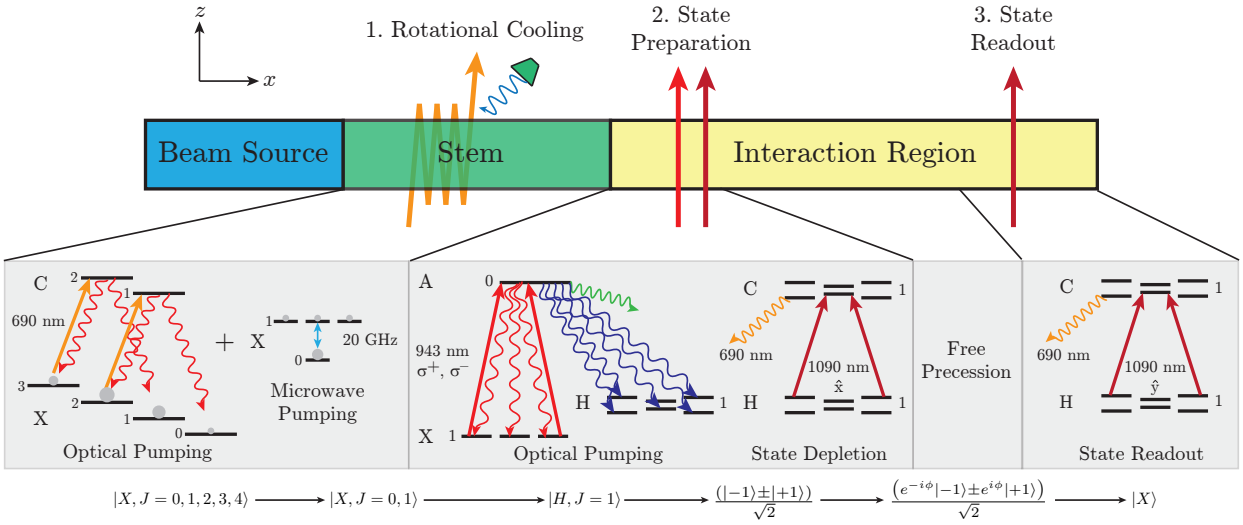

FIG. 1. Schematic of the experimental apparatus used in Gen. 1 of ACME. The relevant molecular transitions are illustrated and written below the corresponding apparatus elements. The y-axis is vertical in the lab. Note that $|-1\rangle$ ($|+1\rangle$) refer to states of the magnetic sublevel M. See main text for a complete description.

rotational population contained in the $J = 0$–4 levels.

Immediately after the beam source the molecules undergo rotational cooling. Laser light addressing the $|X, J = 2\rangle \rightarrow |C, J = 1\rangle$ and $|X, J = 3\rangle \rightarrow |C, J = 2\rangle$ transitions at 690 nm is combined and retroreflected ≈ 7 times. The polarisation of the light is circular and alternates in handedness. The result is that molecular population accumulates in the $|X, J = 0, 1\rangle$ levels. During this optical pumping process microwaves are applied from an *ex vacuo* horn, resonantly coupling the $|X, J = 0\rangle$ and $|X, J = 1, M = 0\rangle$ levels with radiation at $\approx$20 GHz. The microwaves equilibrate population between these two levels, and lead to an extra increase of the population in the $|X, J = 1\rangle$ manifold. These processes occur with a $\approx$50 V/cm electric field applied in the $\hat{y}$ direction. This provides a quantisation axis and also splits the $|X, J = 1\rangle$ M sublevels to aid the microwave pumping. After leaving this region, the lack of a quantising field allows these sublevels to mix incoherently.

Next the molecule beam enters the EDM interaction region where parallel uniform electric and magnetic fields $\vec{\mathcal{E}}, \vec{\mathcal{B}}$ are applied. The molecules are prepared in a pure quantum state, with their inter-atomic axis vector $\hat{n}$ orientated with or against $\vec{\mathcal{E}}$ and with total angular momentum orthogonal to $\vec{\mathcal{E}}||\vec{\mathcal{B}}$. This procedure happens in two stages. First, molecules are optically excited from the $|X, J = 1, M = \pm 1\rangle$ states to $|A, J = 0\rangle$ by laser light at 943 nm. From this state they can then spontaneously decay to the $|H, J = 1\rangle$ manifold. The fraction of population transferred to this state was found to be $\approx 30\%$ by fluorescence measurements. The remaining population decays to other electronic/vibrational states. Within the $|H, J = 1\rangle$ manifold Ω-doubling produces a total of six states with $M = -1, 0, +1$. An electric field mixes $M = \pm 1$ sublevels of the opposite parity Ω-doublets to produce mixed parity states which we label with $\mathcal{N} = \Omega M = -1(+1)$ for the upper (lower) doublet. Of these six states, five are populated from spontaneous emission — the decay $|A, J = 0\rangle \rightarrow |H, J = 1, M = 0, p = +1\rangle$ is forbidden by parity (p). Following this optical pumping process we wish to prepare the spin-aligned state $|H, J = 1, \mathcal{N}\rangle\, 1/\sqrt{2}\,(|M = -1\rangle \pm |M = +1\rangle)$. We drive the $H \rightarrow C$ electronic transition with light at 1090 nm polarised along $\hat{x}$ or $\hat{y}$, and tuned to account for Stark shifts in the levels. This light addresses only the $1/\sqrt{2}(|H, J = 1, \mathcal{N}\rangle\,(|M = -1\rangle \pm |M = +1\rangle) \rightarrow |C, J = 1, M = 0, p\rangle$ transitions respectively; the orthogonal superposition of H state M sublevels is dark (not excited by the laser), and $M = 0$ sublevels are not in resonance with the laser. Hence we deplete the associated population and prepare the dark superposition state $1/\sqrt{2}(|H, J = 1, \mathcal{N}\rangle\,(|M = -1\rangle \mp |M = +1\rangle) \equiv |\psi_\mathrm{i}\rangle$ as a pure initial state. After this step there remains population in the states of opposite $\mathcal{N}$ and in $|H, J = 1, M = 0, p = -1\rangle$, however these states are not in resonance with the lasers and hence ignored.

This initial aligned state then traverses a distance $L \approx 22$ cm. During this time, the angular momentum precesses due to the combined torques of the $\mathcal{B}$-field on the magnetic moment $\mu \equiv g_{H,J=1}\mu_\mathrm{B}$ ($g_{H,J=1}$ is the g-factor for the subscripted state) and the effective electric field $\mathcal{E}_\mathrm{eff}$ on the eEDM, d_e. The wavefunction evolves to $1/\sqrt{2}(|H, J = 1, \mathcal{N}\rangle\,(e^{-i\phi}\,|M = -1\rangle \mp e^{i\phi}\,|M = +1\rangle) \equiv |\psi_\mathrm{f}\rangle$, corresponding to a rotation of the spin-alignment in the xy plane by an angle ϕ. We measure

$$\phi = \int_0^L \left(d_e \mathcal{E}_\mathrm{eff} \mathcal{N} \hat{E} + \mu |\vec{\mathcal{B}}| \hat{\mathcal{B}}\right) \frac{\mathrm{d}x}{\hbar v}, \qquad (1)$$

(x is the axis along which the molecules propagate).

This precession phase is governed primarily by the applied $\vec{\mathcal{B}}$. If there is an eEDM the alignment will be slightly modified depending on the choice of $\mathcal{N}$, thus contributing an eEDM-associated phase, ϕ_e. The detection of this phase is achieved by reprojecting the spin, e.g. onto the axes defined by the initial state preparation. Laser light at 1090 nm addresses both $1/\sqrt{2}(|H, J = 1, \mathcal{N}\rangle (|M = -1\rangle \pm |M = +1\rangle) \equiv |\psi_{x,y}\rangle$ via switching of the polarisation at 100 kHz. This rate ensures all molecules are addressed by both of the $1/\sqrt{2}(|M = -1\rangle \pm |M = +1\rangle)$ quadratures. The associated fluorescence resulting from decay from $|C\rangle$ to $|X\rangle$ is collected and detected. We form an asymmetry, $A = (\langle\psi_x|\psi_f\rangle^2 - \langle\psi_y|\psi_f\rangle^2)/(\langle\psi_x|\psi_f\rangle^2 + \langle\psi_y|\psi_f\rangle^2) = \cos 2\phi$ which is immune to the significant fluctuations in total molecule number which occur on significantly longer timescales. In an ideal case, the shot-noise-limited statistical sensitivity of our eEDM measurement is given by

$$\delta d_e = \frac{\hbar}{2\tau \mathcal{E}_{\text{eff}} \sqrt{\dot{n} T}}, \tag{2}$$

where τ is the coherence time given by the mean molecule forward velocity divided by precession length, $\dot{n}$ is the time derivative of the detected molecule number, and T is the integration time.

B. Gen. 2

A schematic for Gen. 2 is shown in Figure 2. The cryogenic buffer gas beam source is modified for Gen. 2 such that it is based on a thermochemical process, rather than purely ablation.

As in Gen. 1 the molecules are next rotationally cooled, however this scheme will be changed significantly due to the subsequent electrostatic focussing region. For Gen. 2 the population is transferred to $|X, J = 2, M = 0\rangle$. This is an electric weak-field-seeking state for which the electrostatic lens is expected to perform most efficiently. This transfer is achieved by first optically pumping as in Gen. 1, driving the $|X, J = 2\rangle \rightarrow |C, J = 1\rangle$ and $|X, J = 3\rangle \rightarrow |C, J = 2\rangle$ transitions, accumulating population in $|X, J = 0, 1\rangle$. A third laser will then drive the $|X, J = 1\rangle \rightarrow |C, J = 1\rangle$ transition with alternating linear polarisation, pumping population into the $|X, J = 0\rangle$ state. From here, population is transferred to $|J = 2, M = 0\rangle$ via STIRAP.

After rotational cooling, an electrostatic lens is used to counteract the divergence of the molecular beam and enhance the number of molecules which pass into the interaction region. Following the electrostatic focussing the reverse STIRAP process is performed so that the molecules are in a state immune to diabatic state remixing. Within the interaction region the method of state preparation is improved. In Gen. 2, the incoherent process of optical pumping and state depletion will be replaced by coherent STIRAP transfer from $|X, J = 0\rangle$ to $1/\sqrt{2}(|H, J = 1, \mathcal{N}\rangle (|M = -1\rangle \pm |M = +1\rangle)$, thus directly preparing the desired coherent superposition of magnetic sublevels. In order to guard against systematics associated with this STIRAP procedure the molecules are subjected to another laser following the state preparation, which serves to deplete a small undesired state amplitude. This 'refinement' laser beam is identical to the Gen. 1 state preparation beam, and reprojects the desired superposition state.

We plan on keeping the original detection scheme for Gen. 2 of the ACME experiment. However, improvements to the fluorescence collection/detection apparatus, and the possibility of performing optical cycling are discussed in Sections V A and III D respectively.

III. SIGNAL UPGRADES: DISCUSSION AND PRELIMINARY TESTS

In this section we shall discuss the areas of the experimental procedure which can be improved so as to increase the useful molecule flux. We shall outline the factors to consider associated with the possible improvements and present preliminary tests which have been carried out.

A. Rotational Cooling and Zeeman Pumping

Molecules exiting the buffer gas beam source have a rotational temperature of around 4 K; 95% of molecules are in $J = 0, 1, 2, 3, 4$. To maximise usable molecule number we concentrate population in a single rotational level. In Gen. 1 we accumulated population in $|X, J = 1\rangle$, followed by optical pumping via $|A, J = 0\rangle$ into the $|H, J = 1\rangle$ EDM state. As described in Sections III B and IV B we require population in an electric weak-field-seeking state to perform electrostatic focussing. In particular, $|X, J = 1, M = 0\rangle$ was used for preliminary tests, and we plan on using $|X, J = 2, M = 0\rangle$ for Gen. 2.

The scheme used in Gen. 1 is shown in Figure 3. There are two stages: first, a linearly polarised 690 nm laser beam drives the $|X, J = 2\rangle \rightarrow |C, J = 1\rangle$ transition, pumping population from $J = 2$ into $J = 0$. The laser beam is retroflected ≈ 7 times, extending the interaction time with the laser. Driving these transitions with a single polarisation results in a dark state and the small magnetic moment of the X prevents Zeeman remixing. We use a quarter-wave plate to alternate the laser polarisation so all M sublevels are addressed. This stage is carried out without an electric field present. The dependences of the rotational cooling efficiency on the laser power and configuration are shown in Figure 4. We see the expected increase and saturation as the power is increased, and an increase in efficiency when using multiple passes, and using alternating polarisation. The maximum efficiency observed is around 75% of the theoretical maximum.

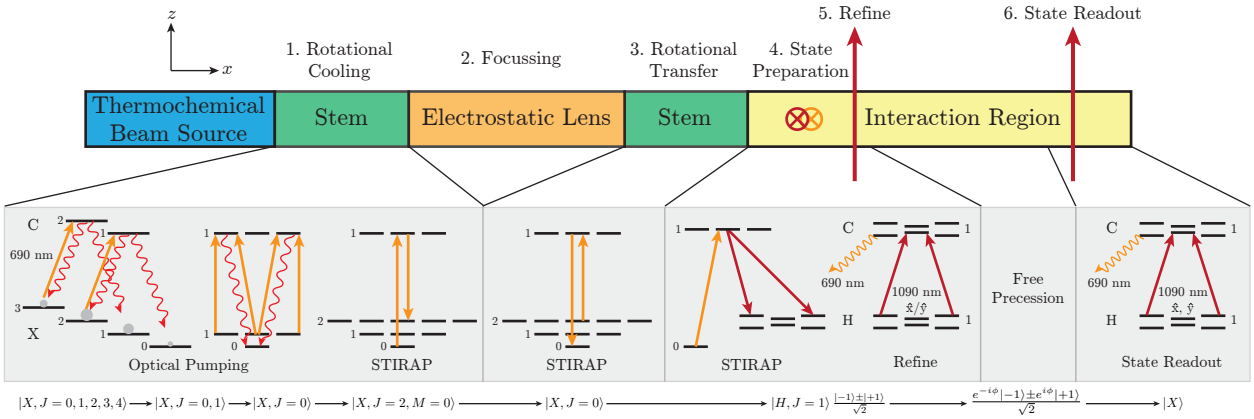

FIG. 2. Proposed experimental scheme for Gen. 2 of the ACME experiment. As with Figure 1 the main sections of the apparatus and associated transitions are shown. See main text for complete description.

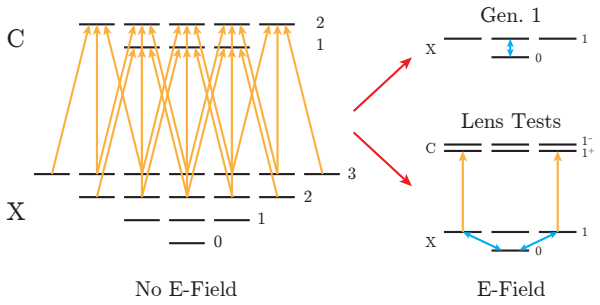

FIG. 3. Rotational cooling scheme used in Gen. 1, as well as the scheme used during preliminary tests of electrostatic lensing. Stark shifts have been omitted for clarity. The left hand side omits Ω-doublets for clarity.

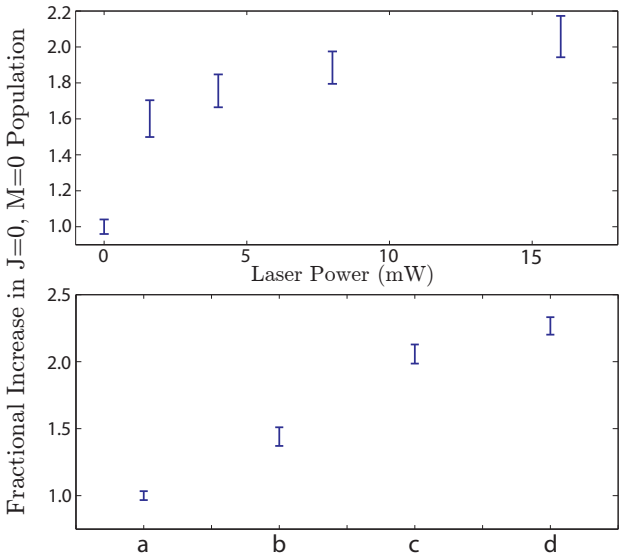

FIG. 4. Upper: Fractional increase in the $|J = 0, M = 0\rangle$ state as a function of laser power driving $|X, J = 2\rangle \rightarrow |C, J = 1\rangle$. Lower: Fractional population increase for a) No pumping, b) Single pass optical pumping, c) Multiple pass, d) Multiple pass with alternating polarisation.

We shall consider the second stage in more detail. Ideally we wish to transfer all population from $J = 0$ into $J = 1$. This can be achieved as follows: a third 690 nm laser, polarised in y, drives the $|X, J = 1, M = \pm 1\rangle \rightarrow |C, J = 1, M = \pm 1\rangle$ transitions. The $|J = 1, M = 0\rangle \rightarrow |J' = 1, M' = 0\rangle$ transition is forbidden, and is anyway not resonant due to Stark splitting from a quantisation field (≈ 50 V/cm orientated along $\hat{y}$). Population accumulates in the dark $|X, J = 0, M = 0\rangle$ state. At the same time we apply linearly polarised microwaves (frequency ≈ 20 GHz) to equilibrate population between $|X, J = 0\rangle$ and $|X, J = 1, M = \pm 1\rangle$. The $|X, J = 1, M = 0\rangle$ state is then dark, and accumulates population. However, measurements showed that implementing this scheme in fact caused the molecule signal to decrease. This is due to the significant (estimated $\approx$ 25%) branching ratio to other vibrational and electronic states from the C state. These losses outweigh the benefits of optical pumping. Instead, we chose to simply apply microwaves on the $|X, J = 0\rangle \rightarrow |X, J = 1, M = 0\rangle$ transition, equilibrating the population between the two sublevels.

Whilst the 'ideal' rotational cooling scheme was not useful for Gen. 1, it was used for preliminary tests of the electrostatic lens, where population had to be accumulated in the $|X, J = 1, M = 0\rangle$ weak-field-seeking state, and so was studied in more detail. The quantising field applied during the $|X, J = 1, M = \pm 1\rangle \rightarrow |C, J = 1, M = \pm 1\rangle$ transition (bottom right of Figure 3) Stark splits the $|X, J = 1, M = 0\rangle$ and $|X, J = 1, M = \pm 1\rangle$ states such that they are resolvable by lasers. However the field should be small to minimise mixing of the opposite parity Ω-doublets which leads to decay from $|C, J = 1\rangle$ to $|X, J = 0, 2\rangle$. In general:

$$|\eta, f\rangle = \cos\theta/2\,|\eta, P^-\rangle - \sin\theta/2\,|\eta, P^+\rangle\,, \qquad (3)$$

where η is a placeholder other quantum numbers

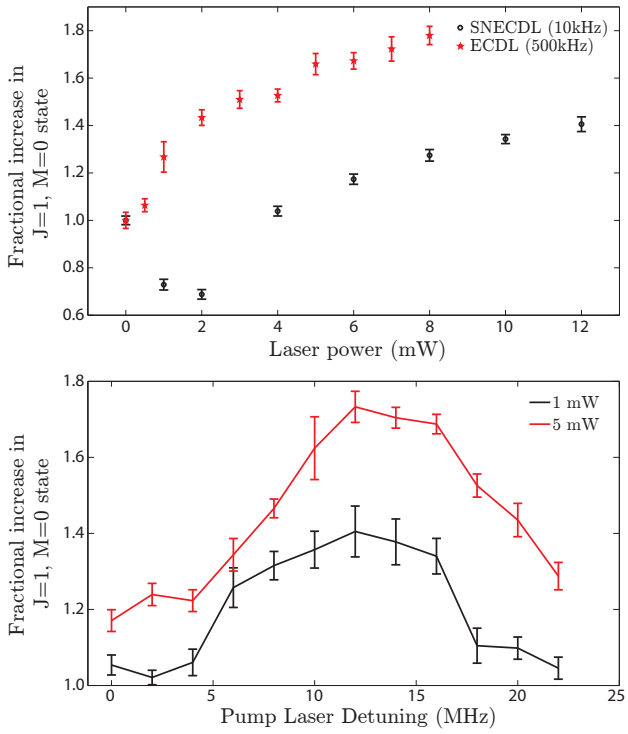

FIG. 5. Top: $|C, J = 1, M = 0\rangle$ population increase whilst driving $|X, J = 1, M = \pm 1\rangle \rightarrow |C, J = 1, M = \pm 1\rangle$ as a function of laser power, for a standard ECDL and a 'self-narrowed' laser (SNECDL). Bottom: Population increase as a function of laser detuning and power.

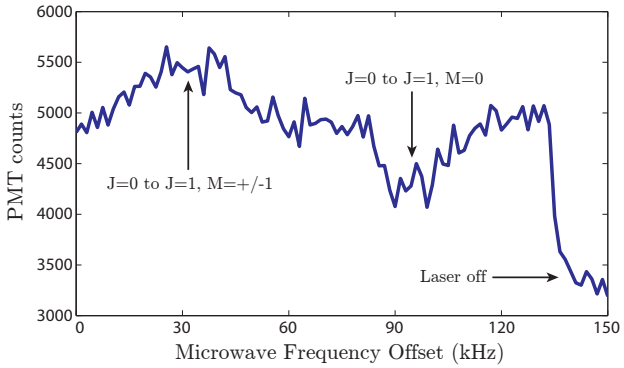

FIG. 6. Fluorescence signal from driving $|X, J = 0\rangle \rightarrow |C, J = 1, M = \pm 1\rangle$ as a function of microwave frequency. Optical pumping is performed on the $|X, J = 1, M = \pm 1\rangle \rightarrow |C, J = 1, M = \pm 1\rangle$ transition, microwaves are polarised orthogonal to the quantising field (corresponding to $|X, J = 0\rangle \rightarrow |X, J = 1, M = \pm 1\rangle$. The signal peak on the left corresponds to microwaves on resonance with $|X, J = 0\rangle \rightarrow |X, J = 1, M = \pm 1\rangle$. The dip in the middle corresponds to the $|X, J = 0\rangle \rightarrow |X, J = 1, M = 0\rangle$ resonance, and the right hand arrow indicates the fluorscence level when optical pumping is not performed.

$(|C, J = 1, M = \pm 1\rangle)$, f labels the lower doublet, $\theta = \arctan(y/x)$, $y = -\mu_{\rm el}\mathcal{E}M\,|\Omega|\,/J(J+1)$, and $x = \Delta_\Omega$ is the zero-field Ω-doublet splitting ($\approx$ 50 MHz). The Stark shift for low fields is quadratic: $\Delta_{\rm St} = \Delta_\Omega^{-1}\left(\mu_{\rm el}\mathcal{E}M\Omega/J(J+1)\right)^2$. We aim to keep $\Delta_{\rm St} < \Delta_\Omega$ and the Ω-doublets relatively unmixed. Calculations and measurements both indicate that efficiency of optically pumping into $|X, J = 1, M = 0\rangle$ only weakly depends on the applied electric field for fields up to 100 V/cm. Measured Stark shifts also yield $\Delta_\Omega = 50.6 \pm 0.7$ MHz and $\mu_{\rm el} = 1.17 \pm 0.03$ MHz/(V/cm) for $|C, J = 1\rangle$.

The dependences of the fractional increase of the $|X, J = 1, M = 0\rangle$ population on laser power, detuning and linewidth are shown in Figure 5. Population increase is measured by driving the $|X, J = 1, M = 0\rangle \rightarrow |C, J = 1, M = \pm 1\rangle$ transition with an additional laser and observing the resulting fluorescence. As expected the population increases with laser power, however there is an unexpected depletion of population when using the narrower laser with low power, observed to be independet of detuning. The effect was not seen with the ECDL over a range of detunings and powers suggesting that the effect is a coherent one; an imperfection in the $\mathcal{E}$-field could allow coupling between $|X, J = 1, M = 0\rangle$ and $|C, J = 1, M = \pm 1\rangle$ leading to a dark state being formed amongst the M sublevels (don't really follow this explanation — Emil?).

Microwave spectroscopy was performed to find the $|X, J = 0\rangle \rightarrow |X, J = 1, M = 0\rangle$ resonance. The electrostatic lens was used to filter out molecules in the weak-field-seeking $|X, J = 0\rangle$ state before driving the aforementioned microwave transition inside a uniform quantising field. The transition $|X, J = 1, M = 0\rangle \rightarrow |C, J = 1, M = \pm, f\rangle$ was then probed with a laser. The observed resonance linewidth was 8 kHz, limited by transit-time broadening. Varying the quantising field reproduces the expected quadratic Stark shift and allows for the electric dipole moment of the X state to be extracted: $d_X = 2.754 \pm 0.047$ D, consistent with theory and an alternative measurement [8, 9]. The field-free transition frequency is extrapolated as $19\,904\,481.4 \pm 1.8$ kHz.

When driving the $|X, J = 0\rangle \rightarrow |X, J = 1, M = \pm 1\rangle$ transition we must take care to avoid also coupling the $|X, J = 0\rangle \rightarrow |X, J = 1, M = 0\rangle$ transition, as this would deplete population from the latter state. Ensuring orthogonality of quantising field and microwave polarisation is difficult and in fact insufficient due to the finite sizes of the molecule beam and microwave radiation, so instead we rely on the quantising field to split the degeneracy of the M sublevels (whilst minimising mixing of the Ω-doublets) and use a low microwave power so that we can resolve them. This is demonstrated in Figure 6. Although the microwaves are polarised in order to drive the desired $|X, J = 0\rangle \rightarrow |X, J = 1, M = \pm 1\rangle$ transition, we also observe the 'bad' π-transition which depletes $|X, J = 1, M = 0\rangle$. We also note, however, that these two transitions are easily resolvable.

The overall increase in $|J = 1, M = 0\rangle$ population due to the methods decribed in this section was around

a factor of three. We estimate the efficiencies of the $|X, J = 2\rangle \rightarrow |C, J = 1\rangle$ optical pumping, $|X, J = 1\rangle \rightarrow |C, J = 1\rangle$ optical pumping, and microwave pumping to be around 75%, 65% and 80% respectively. Emil: These numbers don't add up — you quote a theoretical maximum fractional increase of 4.3 and an achieved increase of about 2.8, yet $4.3 \times 0.75 \times 0.65 \times 0.80 = 1.7$...

B. Electrostatic Lens

ThO molecules are produced via ablation inside a copper cell at around 15 K. Inside the cell they thermalise with a neon buffer gas and exit through a circular aperture. 2.5 cm downstream they pass through a conical collimator of diameter 6 mm. Measurements of transverse and rotational temperature suggest that thermalisation has occurred by this point. 9 cm further downstream the molecules pass through a second collimator of diameter 10 mm. From here the molecules exit the buffer gas beam source and subtend a solid angle of 0.35 sr (full width at half maximum (FWHM) of the intensity distribution) [5]. Molecules which reach the interaction region must pass through a 1 cm $\times$ 1 cm collimating aperture at a distance of around 1.25 m, corresponding to a solid angle of around 6.5×10^{-5} sr. Thus only around 0.02% of the molecules reach the interaction region. By performing electrostatic focussing [10–13] we can recoup a significant fraction of the lost molecules.

The Stark shift $\Delta E_{\rm St}$ of levels in the $X^1\Sigma$ ground state of ThO is quadratic for low fields: $\Delta E_{\rm St} = -\chi \mathcal{E}^2/2$, where $\mathcal{E}$ is the electric field. The polarizability, χ, for a particular rotational state is given by

$$\chi = \frac{\mu_{\rm el}^2}{B_{\rm r}} \frac{J(J+1) - 3M^2}{(2J-1)(2J+3)J(J+1)}, \tag{4}$$

where $\mu_{\rm el}$ is the electric dipole moment, $B_{\rm r}$ is the rotational constant, J is the rotational quantum number and M is the magnetic sublevel. At higher fields there is significant deviation from this quadratic behaviour and the energy levels reach a maximum deviation, thus defining a maximum potential depth for a given J, M. For a given $J > 0$, the $M = 0$ sublevel provides the deepest potential well. Higher J values provide deeper wells, at the expense of requiring dramatically higher field values to obtain them.

For efficient focussing we desire a radial force $F_r \sim r$ (r is a radial distance) and hence use a quadrupole lens so that $\left|\vec{\mathcal{E}}\right| \propto r$ and $\partial \Delta E_{\rm St}/\partial r \propto r$. The molecular trajectories produced by such a lens can be calculated analytically and behave in a manner analogous to rays in a thick optical lens [15]. For small fields, such that the Stark shift remains quadratic in the field, force is linear and given by $F_r = 8\chi V^2 r/R^4$, where V is the applied voltage ($\pm$) and R is the distance from the lens centre to an electrode surface. We assume here that the field shape is a perfect quadrupole. Performing such an analysis the beam properties at the end of such a lens are given by

$$\begin{pmatrix} r \\ \dot{r}/v \end{pmatrix} = \begin{pmatrix} (r_0 + x\dot{r}_0/v)\cos(aL) + \dot{r}_0/av \sin(aL) \\ \dot{r}_0/v \cos(aL) - (ar_0 + ax\dot{r}_0/v)\sin(aL) \end{pmatrix}, \tag{5}$$

where x is the length of field-free travel before the lens, r_0 is the initial radial position, $\dot{r}_0$ is the initial radial velocity, L is the length of the lens, and $a = \sqrt{8\chi V^2/R^4 m u^2}$ with u the initial forward velocity and m the molecule mass. The condition for collimation is thus

$$L = \frac{1}{a} \arctan\left(\frac{1}{ax}\right). \tag{6}$$

This expression is of course only approximate — it assumes no axial velocity spread and no aberrations due to a deviation from a quadratic Stark shift, deviations of the electrode shape from hyperbolic, and corrections to the electric field due to the finite length of the electrodes. It also assumes an initial point source of molecules. Preliminary simulations that include these effects show that Eqn. 6 is a sensible zeroth order approximation under likely conditions, but that many of these effects (particularly the finite spread of velocities and the finite molecular beam source size) substantially affect the final gain in signal. [11].

Preliminary tests of electrostatic lensing were performed in an auxiliary apparatus and demonstrated a significant increase in molecule signal, shown in Figure 8. For these tests the lens electrodes had length L =45 cm; the electrodes were cylinders with radius $R_{\rm el} = 5$ mm and $R = 10$ mm; and applied voltage $|V| < 5$ kV. These values are smaller than we anticipate to use in the ex-

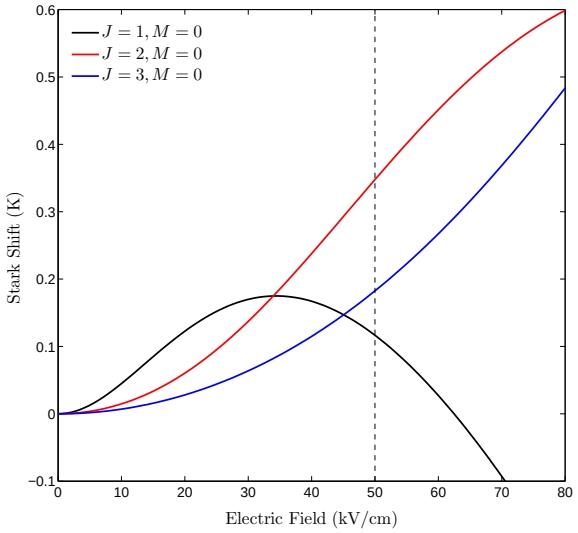

FIG. 7. Stark shifts vs. electric field for the weak-field-seeking $J = 1, 2, 3, M = 0$ levels of the X electronic $^1\Sigma$ state in ThO. We use $\mu_{\rm el} = 2.8$ D and $B_{\rm r} = 0.33$ cm^{-1} [8, 14]. The dashed line indicates the approximate maximum field that we anticipate applying.

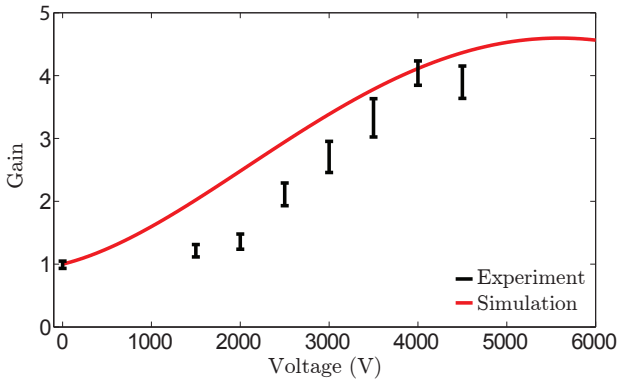

FIG. 8. Molecule signal data from preliminary tests of electrostatic lensing. The gain is the fractional population increase of $|X, J = 1, M = 0\rangle$.

periment proper, due to practical constraints — see Section IV B. For these preliminary tests focussing was performed in the $J = 1$ rotational state. The increase in the molecule signal due to electrostatic focussing under these conditions is shown in Figure 8 An increase of up to a factor of ≈ 4 was observed in the molecule fluorescence when the electrostatic lens was used. The general trend of this gain as a function of applied voltage showed qualitative agreement with Monte Carlo simulation predictions. For the simulation we assume an effective source position 3.6 mm downstream from the cell aperture, of diameter 5 mm; a forward velocity (width) measured to be 160 m/s (40 m/s); and a detection region 25 cm downstream of the cell aperture with transverse cross-section 1 cm^2.

In the full experimental apparatus molecules leaving the electrostatic lens must pass through a collimator before entering the interaction region. Numerical simulations show that molecules passing through this collimator will have a high (close to 100%) chance of performing a diabatic (Majorana) transition to neighbouring M sublevels, leaving them unavailable for later state preparation. This is intuitively expected since molecules passing close to the (conducting) collimators will experience a rapidly varying electric-field direction. Coupled with a relatively small electric-field size, and hence nearby magnetic sublevels, leads to a high chance of spin-changing transitions [16]. Perturbation theory shows the probability of a diabatic transition scales roughly as $P \sim \omega_{\rm rot}^2/\omega_{01}^2$, where $\omega_{\rm rot}$ is the frequency of rotation of the electric field, and ω_{01} is the energy splitting between adjacent M sublevels. Moreover, the probability of these diabatic transitions will depend strongly on their position relative to the collimating edges.

This problem can be circumvented by transferring the molecules from the guided state to the $|J = 0\rangle$ state. When in $|J = 0\rangle$, the nearest state is in $|J = 1\rangle$ — sufficiently far away in energy that diabatic transitions are negligible. This can be achieved by reversing the STIRAP (see Sections III C and IV C) process that we plan to use as part of the rotational cooling in Gen. 2 (Section IV A).

C. State Preparation

In Gen. 1 the EDM state, $|H, J = 1, \mathcal{N}\rangle / \sqrt{2}\,(|M = -1\rangle \pm |M = +1\rangle)$, was prepared via optial pumping — an inherently inefficient process. Molecules that have been rotationally cooled into $|X, J = 1\rangle$ are addressed by a circularly polarised retroreflected laser at 943 nm. This drives two out of the three magnetic sublevels to $|A, J = 0\rangle$, from which they spontaneously decay to $|H, J = 1\rangle$ with an estimated branching ratio of 30%. Decay to each magnetic sublevel is equally likely, with the transition to the odd parity Ω-doublet $|H, J = 1, M = 0\rangle$ state forbidden. Two of the magnetic sublevels of a particular Ω-doublet are then prepared in the desired superposition. Taking all of these factors into account we estimate the efficiency of this process, assuming perfect optical pumping, to be: $2/3 \times 3/10 \times 2/3$ (two out of three sublevels in H) $\times$ $1/2$ (one Ω-doublet) $\times$ $1/2$ (one superposition) $= 1/30$. Given the near-unity efficiency of STIRAP we should be able to gain an order of magnitude in usable molecule number, provided we can rotationally cool as efficiently into a single magnetic sublevel.

We shall consider performing STIRAP from the ground state ($\equiv |1\rangle$) via the $|C, J = 1\rangle \equiv |2\rangle$ state to the EDM state described above ($|3\rangle$). The efficiency of this process depends on a number of criteria. Perhaps the simplest is that for adiabaticity which states that one must satisfy $\Omega_{\rm eff}\tau \gg 1$ where $\Omega_{\rm eff} = \sqrt{\Omega_{12}^2 + \Omega_{23}^2}$ and $\Omega_{12,23}$ are the Rabi frequencies of the pump and Stokes lasers, and τ is the temporal width of the laser pulse sequence. This ensures a slow evolution of the system's eigenvalues compared to their separation [17]. We anticipate $\Omega_{\rm eff}\tau \approx 50$.

Another requirement is that the laser linewidth be small compared to the effective linewidth of the two-photon process in order to achieve an efficient transfer. The two-photon lineshape can be approximated as a Gaussian with halfwidth

$$\delta = 2\Omega_{\rm eff}/\sqrt{\gamma\tau}, \tag{7}$$

where γ is the radiative decay rate of $|2\rangle$, provided $\gamma\tau > 1$ (ACTUALLY $\gg 1$) [18]. Using $D_{12} \approx 0.4\ ea_0, D_{23} \approx 0.02\ ea_0$ [19, 20] we estimate $\delta \approx 2\pi \times 40$ MHz. However, $\gamma\tau > 1$ is not well satisfied for our system: $\gamma = 2\pi \times 0.3$ MHz [19], $\tau \approx 1$ µs. In the opposite limit the two-photon linewidth is determined by Landau-Zener transitions near avoided crossings [21] and the halfwidth is in the range $2\pi \times 200$ kHz$\approx 1/\tau < \delta < 2\pi \times 30$ MHz$\approx \Omega_{\rm eff}$ [18]. Numerical simulations of the optical Bloch equations provide an estimate of δ =VALUE and we require our laser linewidths to be significantly less than this. However, we must also take account of Doppler broadening within the molecular beam; the significant difference between ω_{12} and ω_{23} leads to a significant two pho-

ton detuning. With a Doppler $1/e$ halfwidth (CHECK) $\Delta v \approx 1\ m/s$ the corresponding two-photon linewidth contribution is $\delta_{\text{Dopp}} = \Delta v(\omega_{12} - \omega_{23})/c \approx 2\pi \times 0.5$ MHz. We have tacitly assumed that the single-photon detuning is zero; increasing this reduces the two-photon linewidth [22].

We note in particular that the requirements thus far discussed are all better met with an increase in the Rabi frequency, Ω_{eff}. The ideal STIRAP pulse sequence has peak Rabi frequencies which are matched so we are limited by the Rabi frequency we can supply at 1090 nm ($\approx 2\pi \times 20$ MHz), which has a significantly smaller transition dipole moment.

We also note that more stringent requirements of the spectral purity of the lasers are necessary. Even with the required linewidth, high-frequency phase noise can jeopardise transfer efficiency. Assuming an Ornstein-Uhlenbeck model of laser noise with spectral density D and bandwith G the STIRAP transfer probability, P, can be approximated by [23]:

$$P = \exp\left(-\frac{DG\tau(2G+\gamma)}{4G^2 + 2G\gamma + \Omega_{\text{eff}}^2}\right), \tag{8}$$

in the case of noise uncorrelated between the two lasers (as is the case in our apparatus). Assuming $D = 2\pi \times 10^3$ Hz^2/Hz [24] and $G \to \infty$ (the case of white noise) gives a value of $P = 99.7\%$. If the noise spectral density is significantly larger, in the frequency range of interest ($\gtrsim 1/\tau \approx 1$ MHz), then this can significantly jeopardise transfer efficiency. For example a 100-fold increase would reduce the estimate of P to about 75%, even if the laser linewidth were sufficiently small as discussed above. In contrast to considerations of adiabaticity and two-photon linewidth, this source of transfer inefficiency cannot be suppressed by an increase in Rabi frequency.

A final possible source of inefficiency in the STIRAP transfer is from dephasing between $|1\rangle$ and $|3\rangle$, as such a process would jeopardise the coherence of the 'dark' state, leading to population of the lossy intermediate state. The probability of transfer for a STIRAP sequence which is assumed to be adiabatic, but has a decay rate γ_{31} between the final and initial states, is given by [25]:

$$P = 1/3 + 2/3e^{-3\gamma_{31}\tau/4} \tag{9}$$

if the delay between the laser pulses is the same as their width. Given the fact that the H state is metastable (lifetime= 1.8 ms), the loss due to this dephasing effect can be neglected ($1 - P \approx 0.05\%$).

Initial tests of the STIRAP procedure were carried out in an auxiliary apparatus. The scheme is illustrated in Figure 9 (solid lines). Light at 690 nm and 1090 nm was derived from a pair of self-narrowed ECDLs. For the former wavelength, 10 mW of power was used in the STIRAP beam, whilst the latter was passed through a tapered amplifier to produce around 300 mW of power. This corresponded to a value of $\Omega_{\text{eff}} = 2\pi \times 30$ MHz. (WHAT WAS

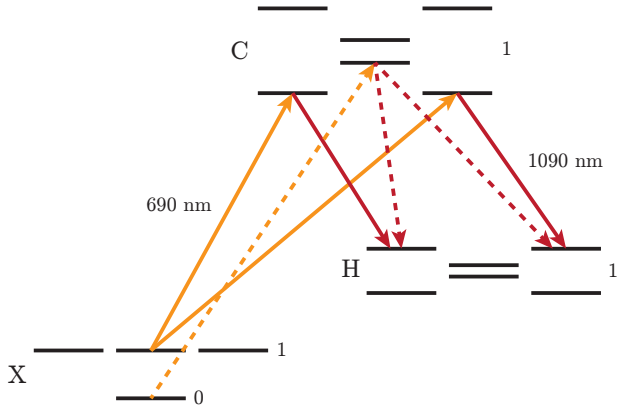

FIG. 9. STIRAP schemes for transferring population from the ground state of ThO to the H state, where our measurement is performed. Solid lines show the transitions used in preliminary STIRAP tests, dashed lines indicate the intended scheme for Gen. 2.

BEAM WIDTH/HEIGHT - VALUE + 1/E? FWHM? WHAT VALUES OF TRANSITION DIPOLE MOMENTS WERE USED?). The 690 nm beam was linearly polarised so as to drive a 'vee' transition, and the 1090 nm beam polarised to drive a π-transition, as shown in Figure 9. The same 1090 nm light was also used to probe the population in the H state downstream by driving the $|H, J = 1\rangle\, 1/\sqrt{2}\,(|M = -1\rangle \pm |M = +1\rangle) \to |C, J = 1, M = \pm\rangle$ transition. The resulting fluorescence at 690 nm due to decay to $|X\rangle$ was observed with a PMT. To assess the improvement in signal this process was compared in quick succession with the optical pumping process $|X, J = 1, M = 0\rangle \to |A, J = 0\rangle$. The dependences of the efficiency of the STIRAP transfer process on the beam powers and two-photon detuning are shown in Figure 10. We see a clear increase in STIRAP efficiency as each of the laser powers is increased, corresponding to a better-met adiabaticity criterion as well as a broader two-photon resonance. It is clear that saturation is not reached for either laser however the data trends, as well as the relative transition strengths, suggest that 1090 nm power is the limiting one. Fitting the two-photon lineshape to a Gaussian yields a FWHM of around 4 MHz. This is significantly smaller than the $>$ 200 MHz predicted by Equation 7 but agrees with the range of values predicted under the assumption that $\gamma\tau < 1$.

With maximum beam powers we observed an approximately six-fold improvement in fluorescence signal. A possible source of error is a relative misalignment of the STIRAP and probe beam directions. This would cause these beams to address different longitudinal velocity classes. As such this amplification factor is considered a lower bound. To circumvent this possible error source we use an alternative detection scheme. An x-polarised 908 nm laser beam was used to address the $|H, J = 1\rangle\, /\sqrt{2}\,(|M = -1\rangle \pm |M = +1\rangle) \to |E, J = 0\rangle$ transition. Population pumped into $|E\rangle$ sub-

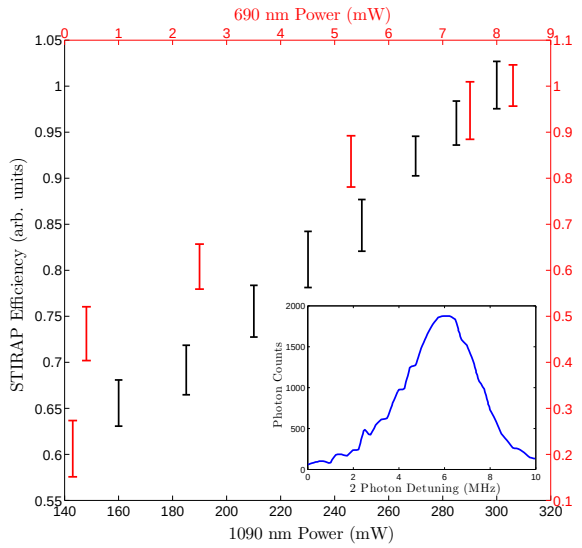

FIG. 10. Dependence of the efficiency of the STIRAP transfer from $|X\rangle$ to $|H\rangle$ on the power in the 1090 nm (690 nm) beam shown in black (red). The inset shows the change in signal as a function of the two-photon detuning. WAS MAXIMUM POWER USED FOR THE OTHER BEAM?

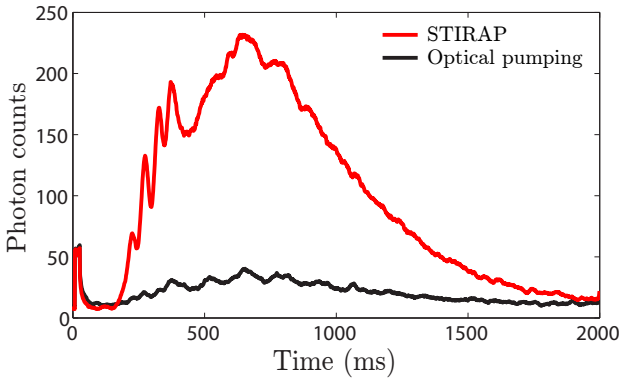

FIG. 11. Comparison of the fluorescence signals obtained when driving the $|H, J = 1\rangle / \sqrt{2}\,(|M = -1\rangle \pm |M = +1\rangle) \rightarrow |E, J = 0\rangle$ transition after both optically pumping and adiabatically transferring population from $|X\rangle$. An approximately eight-fold enhancement in signal was observed.

sequently decays at 613 nm to the $|X\rangle$ state. This laser could then be independently tuned into resonance. (DO YOU NOT ONLY PUMP OUT HALF THE POPULATION WITH THE 908 LASER AFTER OPTICALLY PUMPING WITH 943 THOUGH?).

An extra advantage of this scheme was that it provided sensitivity to the phase between the $|M = -1\rangle$ and $|M = +1\rangle$ levels in $|H\rangle$. Applying a magnetic field parallel to the quantising electric field allowed for tuning and observing the relative phase accumulated, given by

$$\phi = \frac{4\pi}{h} \int_0^L \mu B/v \ \mathrm{d}l. \tag{10}$$

Due to the longitudinal velocity spread of the molecular beam a modulation of the fluorescence signal was observed due to precession of this phase (ARE THESE THE SPIKES ON THE GRAPH? THEY AREN'T VERY REGULAR IF SO). Such an effect is not observed when performing incoherent optical pumping. Comparing the maximum of this fluorescence signal for the case with no net magnetic field with that obtained via optical pumping gave an estimated eight-fold increase in signal, illustrated in Figure 11. By examining both the population in the $|H, J = 1\rangle$ superposition state (accounting for its finite lifetime) and the population remaining in the $|X, J = 1, M = 0\rangle$ state, the efficiency of the STIRAP process was estimated to be 60%. (SO DOES THE FLUORESCENCE SIGNAL LOOKING AT H to C MATCH WITH THE REDUCTION IN SIGNAL LOOKING AT X–¿C THEN? DO YOU ASSUME NO RADIATIVE LOSSES FROM C TO E.G. Q?).

In conclusion we have demonstrated that STIRAP can be used to more efficiently prepare the EDM measurement state; considerations of adiabaticity, phase coherence, and effective addressing of the molecule beam indicate that our system is well suited to an application of this technique and should confer around an order of magnitude increase in usable molecule number.

D. Optical Cycling

IV. GEN. 2 DESIGN

A. Rotational Cooling

Many of the considerations and findings associated with rotational cooling of the moelcule beam were discussed in Section III A where populating the $|X, J = 1\rangle$ level was described. Because we intend to electrostatically focus molecules in the $|X, J = 2, M = 0\rangle$ state, we require a new scheme to achieve this, which is shown in Figure 12 (cf. Figure 1), and proceeds as follows: Molecules exiting the buffer gas beam source will have a rotational temperature of around 4 K, with around 95% of the population in J =0–4. Population in $J = 2$ and $J = 3$ will be depleted via optical pumping by two overlapped laser beams of wavelength 690 nm, addressing $|X, J = 2\rangle \rightarrow |C, J = 1\rangle$ and $|X, J = 3\rangle \rightarrow |C, J = 2\rangle$. These two lasers will be linearly polarised, and retroreflected between a pair of mirrors in order to interrogate the molecule beam multiple times, and ensure maximum depletion of these two states. The beams will also pass through a quarter-wave plate to alternate the chirality of the polarization so all of the magnetic sublevels are addressed.

A second stage of optical pumping follows, whereby molecules in $|X, J = 0\rangle$ are optically pumped into $|X, J = 0\rangle$ via $|C, J = 1\rangle$. This laser, again at 690 nm, will also have alternating polarization. In this case it will

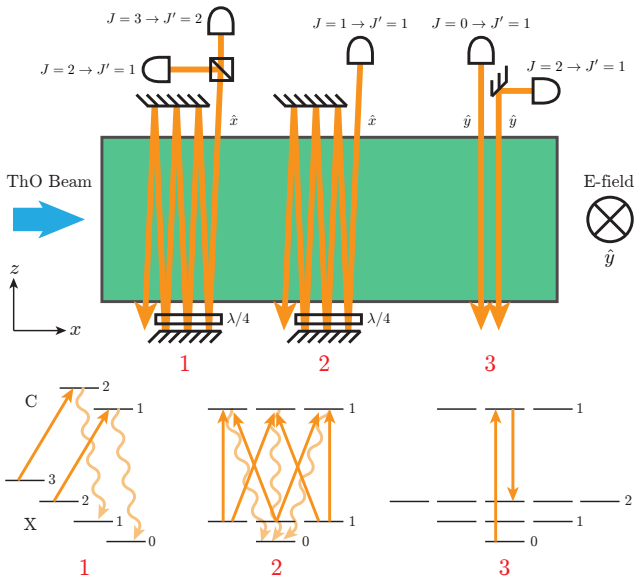

FIG. 12. The intended rotational cooling scheme for Gen. 2. Two stages of optical pumping are applied using three 690 nm laser beams, followed by a STIRAP transfer with two more 690 nm beams. The region shown corresponds to the first 'stem' region (cf. Figure 1). See main text for detailed discussion.

alternate between $\hat{x}$ and $\hat{z}$ linear polarisation. This prevents the formation of dark states within the $|X, J = 1\rangle$ manifold.

With the molecules now in a single magnetic sublevel we can now coherently transfer into $|J = 2, M = 0\rangle$. Two more 690 nm lasers are used to perform STIRAP via the $|C, J = 1, M = 0\rangle$ level. These lasers are significantly narrower than those used for optical pumping, and the necessary considerations associated with STIRAP are discussed in more detail in Section IV C. We note that this particular STIRAP transfer is reversed after electrostatic focusing to transfer back into $|X, J = 0\rangle$ — see Section IV B for further discussion. In this scheme the requirements for a quantising electric field are less stringent than those discussed in Section III A. We require a quantising field for the STIRAP process (orientated in $\hat{y}$), and a field-free region for the first pair of optical pumping processes in order to preserve J selection rules and aid efficiency.

Calculations of the efficiency of this, the Gen. 1, and other rotational schemes were performed, based on a combination of known, exactly calculated, and estimated contributions to the coupling strengths between the various levels. The result is that we estimate the efficiency of the Gen. 1 scheme to be around 35%, i.e. 35% of the molecules produced are transferred to the desired state. This corresponds to a gain in usable molecules of around a factor of 1.8, compared to the case where we do not perform rotational cooling. The scheme for Gen. 2 is predicted to have an efficiency around 25%, however this estimate relies on estimates such as the expected STIRAP transfer efficiency, initial rotational temperature, and the branching ratio from $|C, \nu = 0\rangle \to |X, \nu = 0\rangle$. In particular, if the STIRAP transfer efficiency is as high as 90% then the overall efficiency is predicted to increase to around 40%. Note that the estimated gain is much higher ($\approx$ 4–5) for Gen. 2 as there are significantly fewer molecules initially in $|J = 2, M = 0\rangle$ than in $|J = 1\rangle$, i.e. it is much more important to perform rotational cooling in Gen. 2. Alternative cooling schemes were also considered, which had comparable predicted efficiencies, but were less favourable for practical reasons, e.g. requiring the controlled application of microwaves to the molecular beam.

B. Electrostatic Lens

As described in Section III B, we aim to counteract the divergence of the molecular beam by focussing it with a confining electrostatic potential. Successful incorporation of such a lens into the experimental apparatus must meet a number of criteria. The most important is that a significant gain in the number of molecules transferred to the interaction region is achieved.

Focussing the molecules will also increase their divergence (true collimation of the molecule beam is not possible due to the significant longitudinal velocity spread). As such we must ensure that no molecules impinge on the electric field plates — deposition of ThO would add dielectric material which could cause patch potentials. With increased divergence we must also ensure that we can deliver sufficient laser power to saturate the relevant transitions given the increased spatial and Doppler widths.

We perform Monte Carlo simulations of the beam propagation. As previously described, molecules leaving the cell pass through a 6 mm diameter conical collimator 2.5 cm downstream. We assume that thermalisation proceeds up to this point. Thus the molecules may be travelling in any direction. The initial conditions are then set by considering the trajectories from the conical collimator to the second (10 mm) collimator. The transverse positions and velocities are then determined by this geometry. The axial velocity distribution is assumed to be Gaussian based on measured beam properties (centred at 180 m/s, 30 m/s FWHM). After passing through the rotational cooling region, molecules enter the lens in the $|J = 2, M = 0\rangle$ state for focussing. After exiting the electrodes, the molecules are again transferred to the $|J = 0\rangle$ state by STIRAP, and then travel into the interaction region. The electric field plates have length 42 cm and a short distance in front of them there is a square fixed collimator that protects them from the molecular beam (black line in Figure 13). To perform the simulation we fit a finite-element calculation of the electrostatic potential created by the quadrupole electrodes to a 2D polynomial. We ignore the effect of fringing fields at the begin-

ning and end of the electrodes, i.e. we treat the potential as if it were due to infinitely long electrodes, abruptly beginning and ending at the electrode ends (additional simulations showed such fields have very little effect on the anticipated trajectories, but are important in maintaining adiabaticity).

The optimal parameters were found to be $L = 60$ cm, $R = 1.25$ cm and $V = \pm 20$ kV (we assume 20 kV as a practical maximum to the voltage). The expected trajectories of the molecule beam are shown in Figure 13. Simulations indicate an expected gain of around 20 in molecule number.

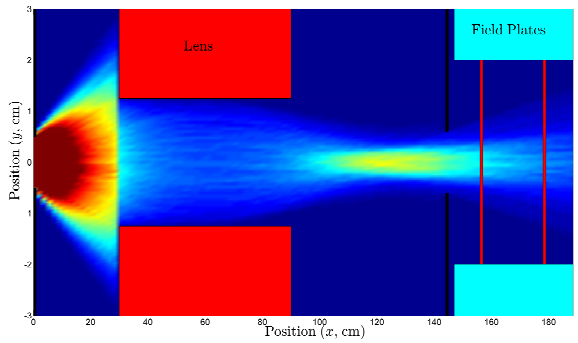

FIG. 13. A sample plot of the computed molecular trajectories for the electrostatic lens. The colourmap shows the distribution of the molecules in one transverse direction, normalised relative to the total number of molecules at that longitudinal position. Note that the distribution in the orthogonal transverse direction is projected, explaining the molecule loss at the lens start. Red rectangles are used to represent the position of the electrostatic lens, blue rectangles show the electric field plate position and black lines show the positions of fixed collimators.

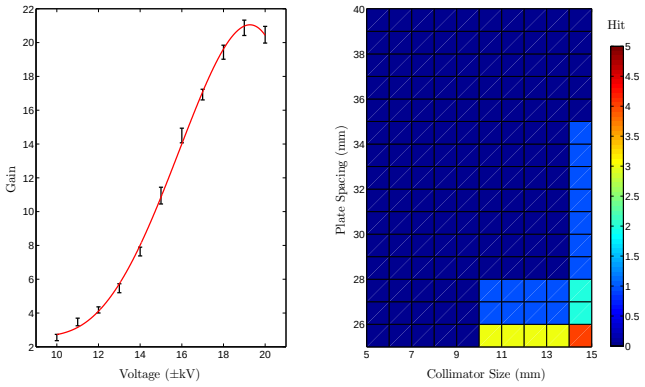

FIG. 14. Left: Molecule number gain provided by the electrostatic lens as a function of the applied voltage. Right: The variation in the number of molecules which hit the field plates, for the same parameters, out of 2,000 trajectories.

In order to ensure that the electrostatic lens would not cause molecules to be deflected onto the electric field plates, a series of simulations was carried out with varying field plate spacing and collimating aperture size. The right-hand side of Figure 14 shows how the number of collisions depends on the collimator size and field plate spacing. We choose values of 12 mm and 40 mm respectively. The chosen configuration ensured that fewer than 1 in 10^8 molecules would collide with the field plates; hence, in a decade of running we should anticipate $< 10^{-5}$ monolayers of ThO molecules would be incident on the field plates.

As previously mentioned, it was also important to verify that the molecule distribution expected in the interaction region still permitted efficient preparation and readout of the molecules. The predicted transverse spatial and velocity distributions of the beam in the detection region each increase by a factor of $\lesssim 2$ due to the focusing. Bearing both of these changes in mind, we must ensure that we can provide a factor of four more laser power to drive these transitions if we wish to saturate them to the same degree as in Gen. 1.

C. State Preparation

After focussing the molecular beam into the interaction region we must prepare the EDM state $|H, J = 1\rangle\, sqrt2\, (|M = -1\rangle \pm |M = +1\rangle)$. As decribed in Section III C this was achieved via optical pumping in Gen. 1 and we plan on replacing this process with STIRAP in Gen. 2. The relevant considerations for this process were considered in Section III C. As described in Section III B, we demand that the molecules is in the $|X, J = 0\rangle$ state as it enters the interaction region to avoid diabatic transitions. Thus the STIRAP scheme planned for Gen. 2 proceeds via the $ketC, J = 1, M = 0$ (negative parity Ω-doublet) state, as shown in Figure 9. We choose to send the STIRAP beams along the $\hat{y}$ direction (aligned with gravity) between the field plates as this will remove scatter due to passing through the electric field plates which would contaminate the fluorescence we are trying to detect. Thus the 690 nm (1090 nm) beam will be polarised along $\hat{z}$ ($\hat{x}$). One could also equivalently use $|C, J = 1\rangle / \sqrt{2}\, (|M = -1\rangle \pm |M = +1\rangle)$ as an intermediate state and swap the laser polarisations.

There are some significant differences in the experimental setup compared to that used for the initial tests of the STIRAP procedure. The Doppler width of the molecular beam is anticipated to be significantly larger, due to the electrostatic focussing, with an estimated transverse velocity $1/e$ halfwidth of ≈ 2.8 m/s, corresponding to a two-photon Doppler halfwidth of $\approx 2\pi \times 1.5$ MHz. However we will also have significantly more power (≈ 7 W) available at 1090 nm through the use of a fiber amplifier. The limiting factor is then how narrow the beam waist can be made, made difficult due to the magnetic shielding requiring the beams be focussed from a distance of at least ≈ 0.6 m. As discussed in Section III C we are working in the regime $\gamma\tau < 1$ (γ is the radiative

decay rate from the intermediate state, τ is the transit time through the beams) which implies the two-photon linewidth is analytically estimated to be in the range $2\pi \times 0.1 - 20$ MHz. Numerically solving the optical Bloch equtions gives an estimate of the two-photon linewidth to be around $2\pi \times 20$ MHz.

As discussed in Section IV A we plan on using STIRAP as part of the rotational cooling, and to transfer to the $|X, J = 0\rangle$ state to avoid diabatic losses. This is a more favourable scheme than that we plan to use to prepare the EDM state. Both the pump and Stokes beams drive the $|X\rangle \rightarrow |C\rangle$ transition, whose transition dipole moment is significantly larger than that of $|H\rangle \rightarrow |C\rangle$, providing a much larger Ω_{eff}. Because the two beams are very close in frequency there is almost no Doppler broadening (< 1 kHz) of the two-photon laser linewidth. Thus we anticipate these STIRAP processes to be easier to perform efficiently.

With this change in experimental procedure it is important to fully understand any associated systematics. We already anticipate that replacing optical pumping with STIRAP will introduce new kinds of systematic effects associated with the interference of different terms in the multipole expansion of the molecular transition $|H\rangle \rightarrow |C\rangle$ (e.g. E1, M1, E2 etc.). In attempt to eliminate such systematic effects we plan on using an additional 'refinement' beam to reproject the superposition state after the STIRAP transfer. Preliminary tests have shown that such a beam can effectively suppress artificially-introduced error in the superposition $1/\sqrt{2}\,(|M = -1\rangle \pm |M = +1\rangle)$. This is demonstrated in Figure 15 where the superposition state was prepared following optical pumping with a laser polarisation correlated with the electric field direction; a second beam was then used to reproject and hence 'clean up' the state.

Following the refinement beam we anticipate the experiment to proceed in an identical manner to Gen. 1 — phase precession followed by reprojection of the phase by driving on $|H, J = 1\rangle / \sqrt{2}\,(|M = -1\rangle \pm |M = +1\rangle) \rightarrow |C, J = 1, M = 0\rangle$ in rapid succession, followed by collection and detection of the resulting fluorescence. Some possible improvements to this aspect of the experiment are discussed briefly in the following section.

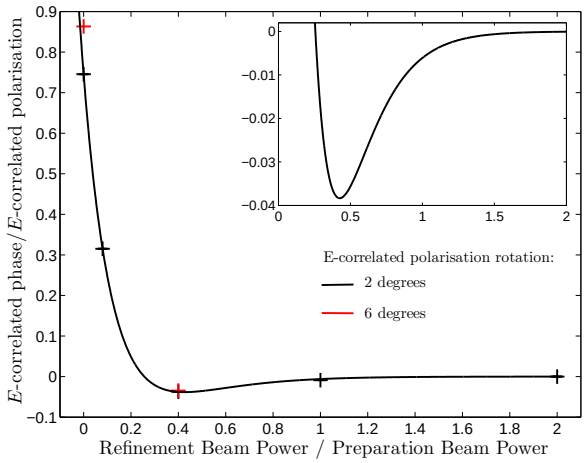

FIG. 15. Data from testing the efficacy of a 'refinement' beam at reprojecting the desired superposition in the $|H\rangle$ state. As the power of this refinement beam is increased the artificially-introduced $\mathcal{E}$-correlated imperfection is efficiently removed. Error bars are smaller than the data points. The fit is a double exponential to guide the eye. Inset shows a zoomed in region of the data fit.

V. OUTLOOK AND CONCLUSION

A. Other Future Gains

There are a number of other possible experimental improvements that are likely beyond the scope of Gen. 2. We discuss these briefly here.

We are developing a new type of buffer gas beam source. The current beam source uses pulsed laser ablation of a pressed and sintered ThO_2 ceramic target to form ThO molecules. The new beam source will instead rely on the thermochemical reaction

$$ThO_2(s) + Th(s) \rightarrow 2ThO(g). \tag{11}$$

The precursor used is instead a mixture of ThO and Th. We have demonstrated that significantly higher peak fluxes can be obtained using this method, as shown in Figure 16 and work is ongoing to verify that larger and stable time-averaged molecule fluxes are possible.

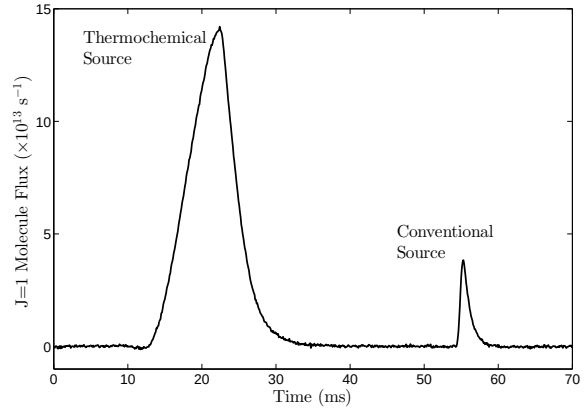

FIG. 16. A comparison of molecule fluxes produced by two different methods. The 'conventional source' corresponds to laser ablation of ThO_2. We observe a fourfold increase in the peak molecule flux.

Perhaps the current biggest limitation to our signal size is the fact that we can only collect at most one photon for each molecule in the interaction region, as the

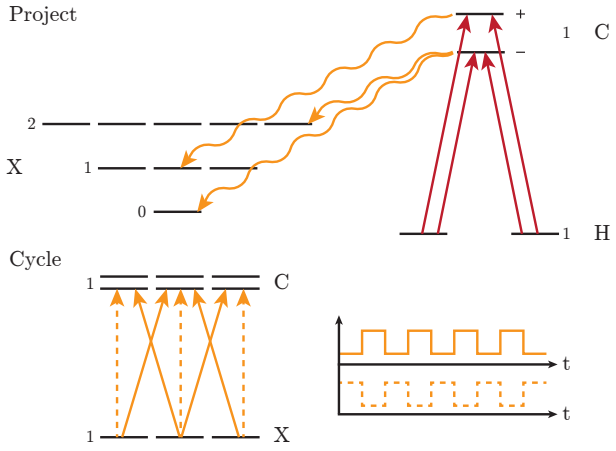

FIG. 17. Outline of an optical cycling scheme. Orthogonal superposition states in H are excited to states of opposite parity in C. These then decay to rotational levels in X of opposite parity, from which optical cycling can be performed. IS POLARISATION SWITCHING NECESSARY HERE?

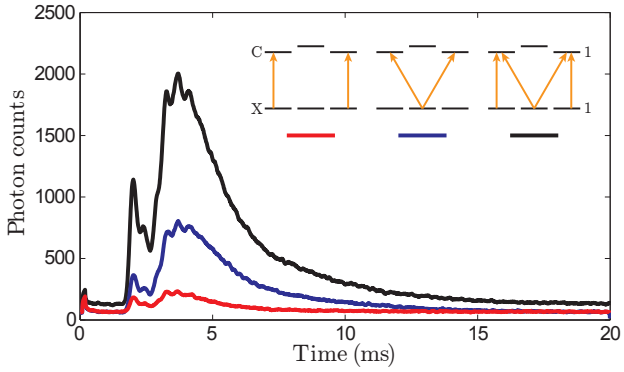

FIG. 18. Data from preliminary tests of optical cycling. Electrostatically focussed molecules are driven on the $|X, J = 1\rangle \rightarrow |C, J = 1\rangle$ transition. Laser polarisation is used to selectively address the M sublevels. The red line corresponds to addressing the $M = \pm 1$ levels, the blue trace to addressing the $M = 0$ level and the black line to alternating between twe two at 200 kHz.

readout procedure transfers all molecules to the ground state, losing the information of the accumulated phase. This inefficiency can be overcome by performing optical cycling. The scheme is illustrated in Figure 17.

In Gen. 1, the orthogonal superposition states $|H, J = 1\rangle / \sqrt{2}(|M = -1\rangle \pm |M = +1\rangle) \equiv |\pm\rangle$ were both read out by exciting to the same state in C. An alternative method for deducing the phase relies on exciting $|\pm\rangle$ to states of opposite parity in C ($|J = 1, M = 0, P = \pm 1\rangle$) [26]. Parity selection rules mean that the subsequent decay projects the populations onto separate rotational levels of X, from which optical cycling can be performed. An optical cycling scheme for the case of population in $|X, J = 1\rangle$ is illustrated at the bottom of Figure 17. We assume incident light polarised along $\hat{x}$ and $\hat{y}$ exciting molecules to the $|C, J = 1, P = +1\rangle$ states. Due to the parity selection rule, decay is back to $|X, J = 1\rangle$, and we can thus cycle the molecules. To avoid population being trapped in dark states of the $|X, J = 1\rangle$ manifold we may apply a quantising electric field along $\hat{z}$ and rapidly switch the light to address the transition with one polarisation at a time. Alternatively, as shown in Figure 17, we can optical pump in zero field and rely on mixing of the M sublevels. The latter approach has the advantage of avoiding any mixing the opposite parity C state Ω-doublets.

The cycling transitions are, however, not perfectly closed. We estimate (CHECK) that around 75% of the population excited to C will decay to the ground vibrational level of X. With lasers just addressing the $|X, \nu = 0\rangle \rightarrow |C\rangle$ we anticipate scattering an average of 12 photons. Repumping out of $|X, \nu = 1\rangle$ increases this number to 90 (WE PROBABLY DON'T TRUST THESE NUMBERS THAT WELL). The number of photons that each molecule can scatter will be limited by the fly-through time. Allowing 1 μs for decay from C (lifetime around 500 ns [26]), a 1 cm beam will permit around 50 photons to be scattered by each molecule. (SAY SOMETHING ABOUT SHOT NOISE? IT IS MULTIPLIED BY 5, SO BECOMES MORE DOMINANT, AND IS FRACTIONALLY REDUCED BY 5).

A preliminary demonstration of the optical cycling detection scheme was performed and demonstrated a significant increase in the gain. Electrostatically focussed molecules were addressed with two lasers addressing the $|X, J = 1, M = 0\rangle \rightarrow |C, J = 1, M = \pm 1\rangle$ and $|X, J = 1, M = \pm 1\rangle \rightarrow |C, J = 1, M = \pm 1\rangle$ transitions. The results are shown in Figure 18. When driving out of $|X, J = 1, M = 0\rangle$ there is significant fluorescence as expected. Driving out of $|X, J = 1, M = \pm 1\rangle$ gives a small amount of fluorescence indicating some residual/remixed population. However, when both transitions are alternately driven the resulting fluorescence is around twice the sum of that for the individual transitions, clearly indicating that optical cycling is taking place. WHY IS THE GAIN SO SMALL? FOR 25% LOSSES TO DARK STATES WE EXPECT TO SCATTER 12 PHOTONS.

Another limitation to our experimental procedure is the efficiency with which we collect and detect the molecule fluorescence. We estimate that around 10% of the fluoresced photons are collected, and the quantum efficiency of the PMTs we is also around 10%.The collection may be improved with a redesigned fluorescence collection setup, such as replacing the current set of collection lenses with a mirror-based setup. The detection may be improved by switching the detection device to an amplified photodiode or hybrid photodetector, which would have a higher quantum efficiency. We are also investigating the possibility of readout via excitation to a higher energy state which would give shorter wavelength fluorescence which typically has a higher associated quan-

tum efficiency.

B. Expected gain

Through theoretical investigation and experimental demonstration we have shown a number of ways in which we expect to improve the statistical sensitivity of the ACME search for the electron EDM. We anticipate that incorporating an electrostatic lens and performing coherent state preparation will both confer a roughly tenfold increase in signal. Since the statistical sensitivity to the electron EDM scales as the square root of the signal this corresponds to an order of magnitude improvement in sensitivity per $\sqrt{\text{day}}$. Thus we hope to either reduce the upper bound on the electron EDM by a similar amount as our previous result, stringently restricting the viable parameter space for some standard model extensions, or achieve the first ever measurement of a non-zero electron EDM.

Looking beyond Gen. 2, there are a number of further improvements, some of which have been partially demonstrated, which could give significant further signal improvement. We believe that a further factor of 10 in signal can be gained by implementing a thermochemical beam source, or optical cycling. In addition, two- or three-fold improvements may be possible by improving fluorescence collection and detection. Combining all possible improvments we conservatively estimate being able to reduce the upper limit on the eEDM value by a factor of 100.

VI. ACKNOWLEDGMENTS

We thank John Barry and David Rahmlow for technical assistance. This work was supported by NSF.

[1] J. Baron, W. C. Campbell, D. DeMille, J. M. Doyle, G. Gabrielse, Y. V. Gurevich, P. W. Hess, N. R. Hutzler, E. Kirilov, I. Kozyryev, B. R. O'Leary, C. D. Panda, M. F. Parsons, E. S. Petrik, B. Spaun, A. C. Vutha, and A. D. West, Science **343**, 269 (2014).
[2] I. B. Khriplovich and S. K. Lamoreaux, *CP Violation Without Strangeness* (Springer, 1997).
[3] E. Commins, Advances in Atomic, Molecular, and Optical Physics **40**, 1 (1999).
[4] A. N. Petrov, L. V. Skripnikov, A. V. Titov, N. R. Hutzler, P. W. Hess, B. R. O'Leary, B. Spaun, D. DeMille, G. Gabrielse, and J. M. Doyle, arXiv (2014).
[5] N. R. Hutzler, M. F. Parsons, Y. V. Gurevich, P. W. Hess, E. Petrik, B. Spaun, A. C. Vutha, D. DeMille, G. Gabrielse, and J. M. Doyle, Physical Chemistry Chemical Physics : PCCP **13**, 18976 (2011).
[6] N. R. Hutzler, H.-I. Lu, and J. M. Doyle, Chemical Reviews **112**, 4803 (2012).
[7] J. F. Barry, E. S. Shuman, and D. Demille, Phys. Chem. Chem. Phys. **13**, 18936 (2011).
[8] A. A. Buchachenko, The Journal of Chemical Physics **133**, 41102 (2010).
[9] F. Wang, A. Le, T. C. Steimle, and M. C. Heaven, Journal of Chemical Physics , 031102 (2011).
[10] H. Bennewitz, W. Paul, and C. Schlier, Zeitschrift fr Physik **141**, 6 (1955).
[11] J. J. Everdig, A. Huijser, and N. F. Verster, Rev. Sci. Instrum. **44**, 721 (1973).
[12] J. Reuss, "State selection by non-optical methods," in *Atomic and Molecular Beam Methods*, edited by G. Scoles (Oxford, 1988) p. 276.
[13] D. Cho, K. Sangster, and E. A. Hinds, Physical Review A **44**, 2783 (1991).
[14] J. Paulovic, T. Nakajima, K. Hirao, R. Lindh, and P. A. Malmqvist, J. Chem. Phys. **119**, 798 (2003).
[15] R. A. Berg, L. Wharton, W. Klemperer, A. B uchler, and J. L. Stauffer, J. Chem. Phys. **43**, 2416 (1965).
[16] T. E. Wall, S. K. Tokunaga, E. A. Hinds, and M. R. Tarbutt, Phys. Rev. A **81**, 033414 (2010).
[17] J. R. Kuklinski, U. Gaubatz, F. T. Hioe, and K. Bermann, Phys. Rev. A **40**, 6741 (1989).
[18] V. I. Romanenko and L. P. Yatsenko, Opt. Comm. **140**, 231 (1997).
[19] P. W. Hess, *Improving the Limit on the Electron EDM: Data Acquisition and Systematics Studies in the ACME Experiment*, Ph.D. thesis, Harvard University (2014).
[20] B. N. Spaun, *A Ten-Fold Improvement to the Limit of the Electron Electric Dipole Moment*, Ph.D. thesis, Harvard University (2014).
[21] M. V. Danileiko, V. I. Romanenko, and L. P. Yatsenko, Opt. Comm. **109**, 462 (1994).
[22] I. I. Boradjiev and N. V. Vitanov, Phys. Rev. A **81**, 053415 (2010).
[23] L. P. Yatsenko, V. I. Romanenko, B. W. Shore, and K. Bergmann, Phys. Rev. A **65**, 043409 (2002).
[24] E. Kirilov and S. Putterman, Eur. Phys. J. D **54**, 683 (2008).
[25] P. A. Ivanov, N. V. Vitanov, and K. Bergmann, Phys. Rev. A **70**, 063409 (2004).
[26] E. Kirilov, W. C. Campbell, J. M. Doyle, G. Gabrielse, Y. V. Gurevich, P. W. Hess, N. R. Hutzler, B. R. OLeary, E. Petrik, B. Spaun, A. C. Vutha, and D. DeMille, Physical Review A **88**, 013844 (2013).